Energy resolution in a high-pressure gas scintillation proportional chamber

Frederic H. Fahey[a)]
Department of Environmental Sciences and Physiology, Harvard School of Public Health, Boston, Massachusetts 02115

Robert E. Zimmerman and Philip F. Judy
Department of Radiology, Harvard Medical School, Boston, Massachusetts 02115

Richard C. Lanza
Laboratory of Nuclear Science, Massachusetts Institute of Technology, Cambridge, Massachusetts 02141

(Received 18 February 1985; accepted for publication 28 June 1985)

A high-pressure gas scintillation proportional chamber has been designed and constructed to image x and gamma rays for medical applications. The chamber contains 4 atm of pure xenon. Ultraviolet light emitted from excited xenon atoms within the detector is collected by a hexagonal array of seven UV-sensitive photomultiplier tubes, which in turn are separated from the pressurized gas by 1-cm-thick fused-silica windows. A model was used to predict the energy resolution of the device as a function of fill-gas pressure, voltage within the detector, and light-collection efficiency. The energy resolution improved with increasing scintillation region voltage from 17% full width at half maximum (FWHM) at 1.9 kV to 10% FWHM at 3.0 kV for 59.5-keV photons; once above 1.5 kV, there was no improvement with increasing drift voltage. The addition of the signals from the peripheral phototubes to that of the center phototube did not substantially improve the energy resolution of the device. This was because the noise that was present yielded a high correlation between the phototubes; when this noise was incorporated into the model, the energy resolution of the multiphototube system was accurately estimated. The energy resolution of the gas scintillation proportional chamber was found to be superior to the sodium iodide Anger camera at 59.5 keV by a factor of 2. Further improvement can be obtained by increasing the scintillation region voltage and by increasing the light-collection efficiency by moving the scintillation region closer to the phototubes.

I. INTRODUCTION

A gas scintillation proportional chamber (GSPC) has been designed and constructed for imaging x and gamma rays *in vivo*. The GSPC, shown in Fig. 1, is a pressure vessel filled with 4 atm of pure xenon. The gas volume is divided into a drift region at low electric field (50–500 V cm^{-1} atm^{-1}) and a light-emitting gap at a higher electric field (1.5–5 kV cm^{-1} atm^{-1}). The position of a photon interaction within the detector can be determined by obtaining the weighted sums of signals from an array of photomultiplier tubes (PMT's). Fused-silica windows separate the gas volume from the PMT array. The spatial resolution and the detection efficiency of this device have been described in other reports.[1,2]

The processes leading to the formation of the GSPC signal are summarized in Fig. 2. When a photon interaction within the drift region produces ionization, the electrons liberated drift in the drift field toward the scintillation region, where the electric field is such that they attain sufficient energy between collisions to excite but not ionize the xenon atoms. The detector operates in the ionization chamber mode, rather than in the proportional counter mode. Each electron traversing the scintillation region excites many atoms, which, upon de-excitation, emit ultraviolet (UV) light. The array of PMT's collects some of these photons, and the location of the scintillation event is estimated.

The number of electrons liberated by the initial ionization is proportional to the amount of energy deposited during the interaction. The statistical variation of this number determines the limit of energy resolution in the gas detector. Each of these electrons leads to the emission of many UV photons from the scintillation region of the GSPC. A fraction of these photons will be collected by the PMT array and it is the variance in the number of these collected photons that defines the energy resolution of the GSPC.

GSPC's have been investigated for use as x-ray telescopes in astronomy,[3,4] and as gamma cameras for imaging radioisotopes, *in vivo*.[5,6] Gas detectors have low quantum efficiency compared to solid-state detectors at photon energies above 100 keV (16% at 140 keV for this GSPC at 4 atm, compared to 90% for a 0.63-cm NaI crystal). Thus their usefulness for imaging is diminished for photon energies above 100 keV. At lower energies, the quantum efficiency for the GSPC is higher (69% at 60 keV).[2] Imaging at these low energies may be useful in nuclear cardiology. The use of thallium-201 for myocardial perfusion studies, and tantalum-178 (9.3-min half-life) and iridium-191*m* (4.9-s half-life) for first-pass cardiac studies, has been investigated.[7–9] All three of these isotopes emit 60–75 keV x rays.

The photons emitted by these isotopes that escape the patient, without interaction, yield the most useful spatial information. A fraction of the emitted photons are scattered within the patient. Some photons from each of these categories pass through a lead, parallel-hole collimator and interact in the detector. The spatial information from the scattered photons is much less than that from the unscattered photons, and some of the former can be eliminated from the image,

 0094-2405/86/010025-10$01.20

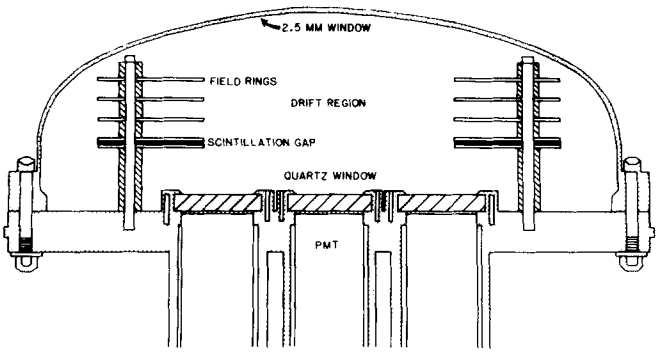

FIG. 1. A cross-sectional view of the GSPC is shown. The chamber consists of a pressure vessel that contains 4 atm of pure xenon. X and gamma rays enter the chamber through a 0.25-cm-aluminum window and interact, generally through the photoelectric event, with the gas atoms in the drift region. The resulting secondary electrons drift in an applied electric field toward the scintillation region. The electric field in the scintillation region is such that the drifting electrons attain sufficient energy between collisions to excite xenon atoms within the region. Upon de-excitation, these atoms emit UV light photons, some of which will traverse the fused-silica windows and be collected by a hexagonal array of seven UV-sensitive PMT's. The energy deposited and the location of the interaction are estimated by appropriate weighted sums of the PMT signals.

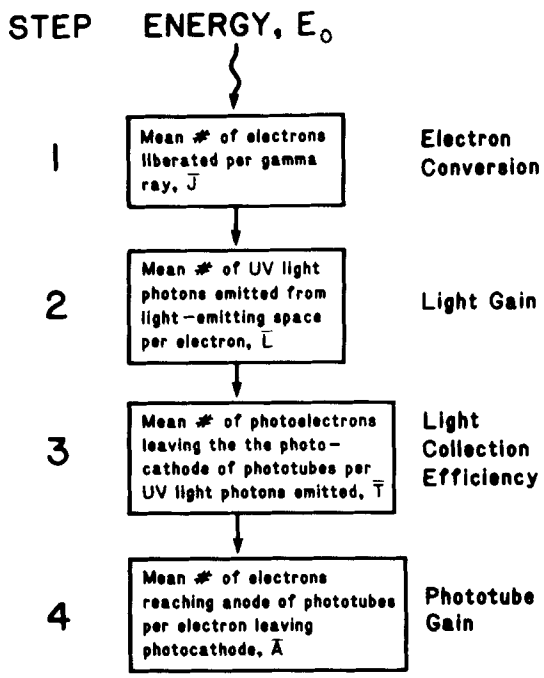

FIG. 2. The secondary scintillation process in the GSPC. (1) The deposition of photon energy E_0 within the chamber yields J secondary electrons drifting toward the scintillation region. The expected value of J is the electron conversion yield $\bar{J}$. (2) Each of these electrons as it traverses the scintillation region of the detector yields the emission of L UV photons. The mean number of UV photons emitted per electron crossing the scintillation region is the light gain $\bar{L}$. (3) A fraction of these emitted UV photons will be collected by an array of UV-sensitive PMT's. The probability that a UV photon emitted from the scintillation region will yield a photoelectron leaving a photocathode of one of the PMT's is light-collection efficiency $\bar{T}$. (4) For each photoelectron leaving the photocathode of the PMT, a large number of electrons will reach the anode of the PMT. The mean of this number, $\bar{A}$, is referred to as the PMT gain.

since Compton scattering also reduces the energy of the interacting photon. In this way, energy discrimination will lead to a higher quality image. This effect has been investigated with respect to the use of semiconductor detectors in photon imaging.[10–12] Energy discrimination necessitates the precise measurement of the signal from the radiation detector.

A GSPC that had 30% energy resolution at 5.9 keV was first reported by Charpak and Renard in 1956.[13] Policarpo reviewed the GSPC research up to 1977, but described no devices that were designed for imaging.[14] In 1979, Nguyen Ngoc *et al.* reported construction of an imaging GSPC that had five PMT's and was operated at 1 atm, and demonstrated energy resolution of 5.4% full width at half maximum (FWHM) at 27 keV.[5] This present paper reports on the design and construction of an imaging GSPC that was operated with a higher gas pressure of 4 atm, which increased the quantum efficiency of the detector, thus making it more suitable for imaging photons with energies between 50 and 100 keV. The energy resolution of this device was evaluated to determine whether these results are consistent with a model based on results at lower photon energies and lower gas pressure. The effect of summing the signals from a number of PMT's to obtain pulse height spectra from a multi-PMT GSPC was also investigated.

II. BASIC THEORY

A. Energy resolution for a single-photomultiplier tube gas scintillation proportional chamber

A block diagram demonstrating the four basic processes leading to the GSPC signal is shown in Fig. 2. The GSPC signal resulting from the deposition of photon energy E_0 is given by

$$\bar{S}(E_0) = \overline{JLTA}\,. \tag{1}$$

$\bar{J}$ is the electron conversion yield and is the mean number of electrons liberated per deposition of photon energy E_0. $\bar{L}$ is the light gain of the GSPC, and represents the mean number of UV photons emitted per electron traversing the scintillation region of the detector. The light-collection efficiency $\bar{T}$ is the probability that a UV photon emitted from the scintillation region will lead to the emission of an electron from the photocathode of the PMT of the device. The PMT gain $\bar{A}$ is the mean number of electrons reaching the anode of the PMT per electron emitted from the photocathode. The signal of the GSPC, $\bar{S}$, is the integral under the current pulse from the PMT, which is directly proportional to the number of electrons reaching the anode of the PMT per event.

Energy resolution is the variation in the GSPC signal for an energy deposition of E_0. It is represented as the ratio of the FWHM of the pulse height distribution to the pulse height mean. Each of four stages of this GSPC signal process will be described along with a theoretical expression for its variance. These factors will be combined to obtain the relative variance of the GSPC signal, where the relative variance is the ratio of the variance to the square of the expected value.

1. Electron conversion yield (Figure 2, step 1)

Photons entering the GSPC interact, generally through the photoelectric effect, in the drift region of the detector. The photoelectron proceeds to ionize a number of other gas atoms resulting in an electron swarm that drifts in an electric field (50–500 V cm^{-1}) toward the scintillation region. The number of electrons in this swarm is represented by the value J. Its expected value is referred to as the electron conversion yield, and given by

$$\bar{J} = E_0 / \bar{w} , \tag{2}$$

where $\bar{w}$ is the mean energy expended per ion pair produced. The variance of this value was obtained theoretically due to a formulation by Fano.[15] The distribution of J is Poisson in nature, modified by the Fano factor to take into account the dependence between ionizations. The variance of J is given by

$$\text{var}(J) = F\bar{J} , \tag{3}$$

where F is the Fano factor. Both F and $\bar{w}$ are properties of the detector material. F and $\bar{w}$ have values of 0.15 ± 0.03 and 21.5 eV per ion pair, respectively, for xenon.[16,17]

2. Light gain (Figure 2, step 2)

The scintillation region is at increased electric field relative to the drift region, between 1.5 and 5.0 kV cm^{-1}. Each electron, while traversing this space, excites a number of gas atoms, which, upon de-excitation, emit ultraviolet photons. It has been demonstrated experimentally[18] and shown theoretically[19] that the number of photons emitted per unit distance traveled by the electron is proportional to the electric field, i.e.,

$$\frac{d\Lambda}{dx} = kE_s , \tag{4}$$

where Λ is the number of photons emitted per electron while drifting the distance dx, and E_s is the electric field within the scintillation region. Integrating this equation from 0 to d, the thickness of the scintillation region, yields

$$\begin{aligned} L &= \Lambda(d) \\ &= k(V_s - V_{\text{th}}) , \end{aligned} \tag{5}$$

where V_s is the reduced voltage (voltage normalized by pressure) across the scintillation region, and V_{th} is the threshold reduced voltage for secondary scintillation. Therefore the amount of light emitted per electron in the GSPC is proportional to the voltage across the scintillation region once above the threshold voltage V_{th}. The expected value of L in Eq. (5) is referred to as the light gain and is defined as the mean number of scintillation photons emitted per electron that drifts across the scintillation region.

As the electrons drift across the scintillation region, they can either interact by elastic or inelastic electron scattering, the latter leading to excited, fill-gas atoms. If the inelastic electron scattering events are independent, and the probability for such scattering is constant, then the distribution of L would be Poisson. However, as was the case with the ionization by the photoelectron, these are not independent events. deLima *et al.*[16] have thus used Fano's formulation[15,20] to obtain the variation in light gain,

$$\text{var}(L) = G\bar{L} , \tag{6}$$

where G is a Fano-like factor relating the true variance to that of a Poisson distribution. G is 0.2 for xenon.[16]

3. Light collection efficiency (Figure 2, step 3)

The probability that a UV photon that is emitted from point (x,y,z) within the scintillation region leads to the emission of an electron from the photocathode of the PMT is constant and independent of the consequences of other emitted photons. Therefore the number of electrons emitted from the photocathode per UV photon is described by a binomial distribution. If the probability described above is given by $T(x,y,z)$, then for N photons emitted from the point (x,y,z), the mean number of electrons emitted from the photocathode will be

$$\bar{c} = NT(x,y,z) , \tag{7}$$

and the variance of this value is given by

$$\text{var}(c) = NT(x,y,z)[1 - T(x,y,z)] . \tag{8}$$

Equations (7) and (8) would be true for fixed N; however, N is also a random variable, given by the product JL. To include the fact that there is also variation in N, the following equation must be used:

$$\text{var}(c) = \langle \text{var}(c/N) \rangle_N + \text{var}_N \langle c/N \rangle , \tag{9}$$

where $\text{var}(c/N)$ and $\langle c/N \rangle$ represent the variance and expected values of c with N fixed [given by Eqs. (7) and (8)], and $\langle \rangle_N$ and var_N are the expected value and variance taken over the random variable N, respectively. This equation yields

$$\text{var}(c) = T(1 - T)\bar{N} + T^2 \text{var}(N) , \tag{10}$$

and the relative variance is given by

$$\frac{\text{var}(c)}{\bar{c}^2} = \frac{\text{var}(N)}{\bar{N}^2} + \frac{(1/\bar{N})(1 - T)}{T} . \tag{11}$$

The probability that an emitted photon will yield the emission of an electron from the photocathode of the PMT is referred to as the light-collection efficiency T, and is a function of position because the total photocathode area subtends a different solid angle for each point (x,y,z). In the GSPC, light is emitted along a line segment within the scintillation region that is parallel to the field lines therein. An effective z position can be defined such that all the light is considered to come from this plane. Thus the notation $T(x,y,z_{\text{eff}})$ will be used.

Let the mean efficiency be defined as

$$T = \frac{\int\int T(x,y,z_{\text{eff}})\, dx\, dy}{\int\int dx\, dy} , \tag{12}$$

where the integrations are performed over the area of the scintillation region that is emitting UV photons. If $T(x,y,z_{\text{eff}})$ does not vary substantially over the area being irradiated, then $\bar{T}$ can be substituted into Eqs. (7), (8), and (11). Since a collimated source was used in the experiments being reported, this substitution was made.

4. Photomultiplier tube gain (Figure 2, step 4)

The gain of the phototube is defined in this paper as the number of electrons reaching the anode of the phototube per electron emitted from the photocathode of the PMT. This value is designated by the value A. If each electron incident upon the first dynode leads to the emission of δ electrons towards the next dynode, and there are M dynode stages, then

$$\overline{A} = K_1 \delta^M , \tag{13}$$

where K_1 is a constant.[21] The relative variance of the gain is approximately given by

$$\mathrm{var}(A)/\overline{A}^2 \simeq 1/(\delta - 1) . \tag{14}$$

Combining the separate relative variances, in order to obtain the relative variance of the signal S, yields the following expression:

$$\frac{\mathrm{var}(S)}{\overline{S}^2} = \frac{\mathrm{var}(J)}{\overline{J}^2} + \frac{(1/\overline{J})\mathrm{var}(L)}{\overline{L}^2} + \frac{(1/\overline{JL})(1-\overline{T})}{\overline{T}} + \frac{(1/\overline{JLT})\mathrm{var}(A)}{\overline{A}^2} = \frac{1}{\overline{J}}\left\{ F + \frac{G}{\overline{L}} + \frac{1}{\overline{LT}}\left[1 - \overline{T} + \frac{\mathrm{var}(A)}{\overline{A}^2} \right] \right\} . \tag{15}$$

This formulation was first presented by deLima *et al.*[16] If the light gain $\overline{L}$ is large and the light-collection efficiency $\overline{T}$ and the relative variance of the PMT gain $\mathrm{var}(A)/\overline{A}^2$, are small, then Eq. (15) can be estimated by

$$\mathrm{var}(S)/\overline{S}^2 \simeq (1/\overline{J})[\, F + (1/\overline{LT})\,] , \tag{16}$$

and the variance becomes

$$\mathrm{var}(S) = \overline{JL}^2 \overline{T}^2 \overline{A}^2 [\, F + (1/\overline{LT})\,] . \tag{17}$$

Using reasonably conservative values, such as a light gain value of 50, a light-collection efficiency of 5% and a relative error in the gain of the PMT of 10%, with a Fano factor of 0.17 and a G value of 0.2, the relative variance value obtained using Eq. (16) differs by less than 1% from that of Eq. (15) for a gamma-ray deposition of 60 keV. Equation (16) is used to estimate the energy resolution in subsequent analyses.

B. Energy resolution for the multiphotomultiplier tube gas scintillation proportional chamber

The GSPC uses a hexagonal array of phototubes and Anger-type logic to obtain an image.[22] To determine the energy signal from the GSPC, the signals from the various PMT's are added together on an event-by-event basis. With $\overline{T}_i$ the light-collection efficiency of the ith PMT, $\overline{A}_i$ the gain of the ith PMT, and w_i the weight assigned to the signal from the ith PMT, a weighted sum of the signals from n PMT's can be taken. The result is referred to as the sum signal S_s. The weights are selected according to the task. Certain weights will minimize the variation in the sum signal, while others will make the sum signal as uniform as possible over the field of view of the detector. The expected value and relative variance of the sum signal from n PMT's, added together on an event-by-event basis, are given by

$$\overline{S}_s = \overline{JL} \sum_{i=1}^{n} \overline{T}_i \overline{A}_i w_i , \tag{18}$$

and

$$\mathrm{var}(S_s)/\overline{S}_s^2 \simeq (1/\overline{J})[\, F + (1/\widetilde{LT})\,] , \tag{19}$$

where

$$\widetilde{T} = \left(\sum_{i=1}^{n} \overline{T}_i \overline{A}_i w_i \right)^2 \Big/ \left(\sum_{i=1}^{n} \overline{T}_i \overline{A}_i^2 w_i^2 \right) . \tag{20}$$

These equations are derived in the Appendix. $\widetilde{T}$ is the effective efficiency of the multi-PMT detector. The ratio of $\widetilde{T}/\overline{T}$ describes the efficiency gained by the inclusion of more PMT's into the energy resolution process.

For the best energy resolution, the relative variance should be minimized, which is the case when $\widetilde{T}$ is at its maximum value (for fixed light gain $\overline{L}$, and electron conversion yield $\overline{J}$). This occurs when

$$\overline{A}_i w_i = \overline{A}_j w_j \quad \text{for } 0 < i, j < n , \tag{21}$$

which implies that if the gains of the PMT's are not identical, then in order to optimize energy resolution, the weights should be chosen such that the gain–weight product is equal for all PMT's.

The simplest case is that of unity weights for all PMT's and equal PMT gains. For that case,

$$\widetilde{T} = \sum_{i=1}^{n} \overline{T}_i . \tag{22}$$

Thus adding in more tubes effectively increases the light-collection efficiency. Then $\widetilde{T}$ can be substituted for $\overline{T}$ in Eqs. (1) and (15) to calculate the mean signal and relative variance.

The correlation coefficient of the signals between any two PMT's can also be obtained, and is given by

$$r_{ij} = \frac{F}{[\, F + (1/\overline{LT}_i)\,]^{1/2} [\, F + (1/\overline{LT}_j)\,]^{1/2}} . \tag{23}$$

This equation is also derived in the Appendix. This equation contains no dependence on PMT gain or pulse height. This correlation is caused by simultaneous measurement of the same event by each PMT. It does not, however, include other sources of correlated noise that may be present. Variation in dc level caused by interference would be an example of such noise and if present, the sum signal would not yield as large an improvement in energy resolution relative to the single-PMT system as would be predicted by the above formulation. If V_c represents the variance due to such a source of correlated noise, then the relative variance for the ith PMT is

$$\mathrm{var}(Si)/\overline{S}_i^2 = (1/\overline{J})[\, F + (1/\overline{LT}_i)\,] + V_c/\overline{S}_i^2 ,$$

and the relative variance of the sum signal becomes

$$\mathrm{var}(S_s)/\overline{S}_s^2 = (1/\overline{J})[\, F + (1/\widetilde{LT})\,] + [2(N^2 - N)(V_c/\overline{S}_s^2)] , \tag{24}$$

where N is the number of PMT's. The correlation coefficient between the ith and the jth PMT would then be

$$r_{ij} = \frac{F + \overline{J} V_c/(\overline{S}_i \overline{S}_j)}{[\, F + (1/\overline{LT}_i)\,]^{1/2} [\, F + (1/\overline{LT}_j)\,]^{1/2}} . \tag{25}$$

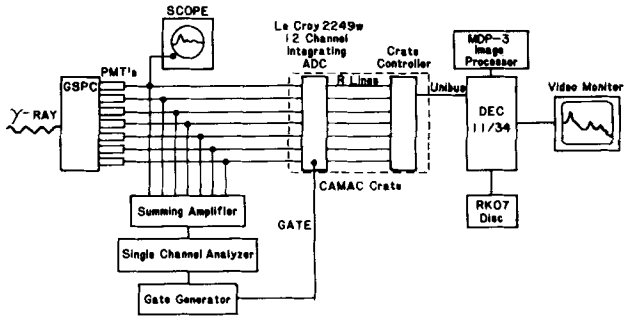

FIG. 3. GSPC electronics block diagram. The signal from each PMT is split, one going to an integrating ADC and the other to a summing amplifier. If the output of the summing amplifier is above a threshold determined by the single channel analyzer, then a gate pulse is generated. Upon reception of a gate pulse, the ADC integrates all of its channels for a period of time equal to the duration of the gate pulse. The resulting digitization is read into computer memory through CAMAC hardware and stored on magnetic disk. Weighted sums of these PMT signals can be obtained and displayed on the video monitor through image processing hardware.

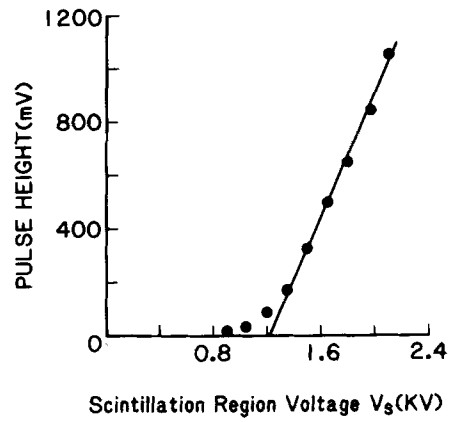

FIG. 4. The pulse height resulting from secondary scintillations within the GSPC as a function of scintillation region voltage is shown. Once above the threshold voltage for secondary scintillation (1.2 kV), the relationship is linear. The drift voltage and the integration time, for these measurements, was kept constant at 2.1 kV and 6 μs, respectively.

III. INSTRUMENTATION

The GSPC, shown in Fig. 1, is a pressure vessel with a 0.25-cm-aluminum entrance window. The chamber is filled with 4 atm of pure xenon that was purified by circulation through hot, calcium turnings. The scintillation region is defined by two stainless-steel meshes, separated by 3.1 mm. The meshes are made up of 0.0025-cm-diam wire with 40 wires/cm (80% open area). Several field-shaping rings keep the field lines in the drift region straight and normal to the mesh planes. The UV scintillation photons are collected by a hexagonal array of seven ultraviolet-sensitive phototubes (Hammamatsu model R208), i.e., one in the center and six on the periphery. The scintillation region is located 5 cm above these PMT's, which are separated from the pressure vessel by 1.25-cm-thick fused-silica windows. These windows transmit approximately 50% of the photons normally incident upon them that have a wavelength of 170 nm (the wavelength of the secondary scintillation photons in xenon).

The electronics associated with this detector are shown in Fig. 3. The signals from the PMT's are split, with one going to a summing amplifier and the other to a 12-channel, integrating analog-to-digital converter (ADC) (LeCroy 2249W). When the output of the summing amplifier exceeded a certain threshold, a rectangular gate pulse was transmitted to the ADC. For each gate pulse received by the ADC, the seven PMT signals were integrated and digitized. The time over which the PMT signals were integrated was determined by the length of the gate pulse, which was easily varied. The ADC was a CAMAC module and was interfaced to a Digital Equipment Corporation (DEC) 11/34 minicomputer by a CAMAC crate and crate controller (Kinetic Systems). The seven digitized PMT signals were read into the 11/34 and subsequently stored on magnetic disk. This was done on an event-by-event basis. The sum signal, as defined in Eq. (18), was obtained by taking the appropriate weighted sum of these stored data. The pulse height spectrum was obtained by forming a histogram from the sum signal values. The spectrum from a single PMT was obtained by weighting the remaining PMT's by zero.

The pulse shape of the PMT signal from this GSPC was Gaussian-shaped with a FWHM of approximately 2 μs and a full width at tenth maximum (FWTM) of 5 μs. The pulse height increased directly with gap voltage once above a threshold voltage of 1.2 kV (Fig. 4). For these reasons, the typical values used in the experiments were 2.2-kV drift voltage (i.e., voltage across the drift region), 2.6-kV scintillation region voltage, 1.45-kV PMT voltage, and 6-μs integration time.

The quantum detection efficiency of this device was 65% at 60 keV.[1] The NEMA (National Electrical Manufacturer's Association) resolution phantom was used to obtain a line spread function (LSF). The intrinsic, spatial resolution of the device was 4.3 mm full width at half maximum of the LSF at 81 keV.[2]

IV. EXPERIMENTAL METHODS

For all of the experiments performed in this study, the photon sources were collimated (2.69×10^{-3} steradians solid angle, yielding a beam diameter less than 1.0 cm at the scintillation region) and the beam was normally incident upon the GSPC entrance window. In order to determine the energy resolution of the chamber, pulse height spectra were obtained from the GSPC for the following isotopes: technetium-99*m* (Tc-99*m*, 140-keV gamma ray), xenon-133 (Xe-133, 81-keV gamma ray, and x rays around 30 keV), and americium-241 (Am-241, 59.5-keV gamma ray). From these spectra, the energy resolution and energy linearity were measured. With the drift voltage at 2.2 kV, the scintillation region voltage at 2.6 kV, and 6-μs integration time, the centroids of each energy peak of interest were plotted as a function of the deposited energy associated with that peak. These data were used to obtain a keV-to-channel number calibration factor.

Pulse height spectra of Am-241 were obtained for a series of different scintillation region voltages, keeping the drift voltage, PMT voltage, and the integration time constant. The energy resolution and the centroid value of the 59.5-keV, full-energy peak were measured and plotted versus

scintillation region voltage. Combining Eqs. (5) and (17) and noting that the variance of the GSPC signal is directly proportional to the square of the energy resolution given as the FWHM, then the following equation is obtained:

$$\text{FWHM}^2 = AV_*^2 + BV_* , \tag{26}$$

where

$$V_* = V_s - V_{\text{th}} ,$$

V_s is the voltage across the scintillation region, and V_{th} is the threshold voltage for secondary scintillation in the GSPC [as in Eq. (5)]. Thus the energy resolution should be related to the scintillation region voltage by a linear quadratic. Experiments were also performed for different drift voltages and integration times.

The inclusion of all seven PMT's into the energy resolution measurement was also investigated. By using measurements of the respective PMT signals and the energy resolution values, the light-collection efficiency and PMT gain of each of the seven PMT's were estimated. These data were used to predict the relative variance of the sum signal according to Eqs. (19) and (20). Although PMT signal value alone cannot separate the effect of PMT gain from efficiency, energy resolution is much more strongly dependent upon light-collection efficiency. This is seen in Eq. (16). In the more complete Eq. (15), there is a term containing PMT gain, but the dependence of energy resolution upon PMT gain due to this term is quite small. Once the energy resolution for a PMT has been measured, one can solve for the light gain–efficiency product $\overline{LT}$, using Eq. (16). Since the effects of the light gain and the light-collection efficiency could not be separated by this method, it was convenient to choose one PMT as a reference and then normalize the $\overline{LT}$ estimates of the other PMT's to this one. This was referred to as the relative light gain–efficiency product and was represented by $(\overline{LT})_{\text{rel}}$. Since the light gain $\overline{L}$ is independent of the PMT number, the relative light-collection efficiency is equal to the relative light gain–efficiency product.

If $P_{\text{rel}}(i)$ is the channel number of the centroid of the peak of interest in the pulse height spectrum for the ith PMT, normalized by the same measurement for the reference PMT, the relative PMT gain $A_{\text{rel}}(i)$ is estimated by dividing $P_{\text{rel}}(i)$ by the relative light-collection efficiency. Utilizing Eq. (21), the weights necessary for optimum energy resolution are obtained by taking the reciprocal of the relative PMT gains. Referring to Eq. (20), the following expression for the relative light-collection efficiency is obtained:

$$\tilde{T} = \frac{\left\{\sum_{i=1}^{n} T_{\text{rel}}(i)\tilde{A}_{\text{rel}}(i)w(i)\right\}^2}{\left\{\sum_{i=1}^{n} \overline{T}_{\text{rel}}(i)\left[\tilde{A}_{\text{rel}}(i)w(i)\right]\right\}^2} . \tag{27}$$

To obtain the absolute expression of the light gain–efficiency product, the relative value must be multiplied by the light gain–efficiency product of the reference PMT, i.e.,

$$\widetilde{LT} = (\overline{LT})T_{\text{rel}} . \tag{28}$$

This estimate for $\widetilde{LT}$ can be substituted into Eq. (19) to obtain the energy resolution of the multi-PMT system.

A single acquisition consisted of storing the seven PMT signals for each of a series of events on magnetic disk. Five separate acquisitions of 20 000 events each were obtained for a collimated Am-241 source. Each acquisition was then analyzed to obtain the pulse height spectra for each of the seven PMT's. The signal from each PMT was estimated by the channel number of the centroid of 59.5-keV peak of Am-241 spectrum. The energy resolution associated with the 59.5-keV peak was also obtained. The mean of the energy resolution and pulse height and their standard errors were then obtained from the five values for each PMT. The light gain–efficiency product was estimated from the mean value of the energy resolution. Using the center PMT as a reference, the relative light gain–efficiency product and signal value were obtained for each PMT. The relative phototube gain of each PMT was estimated, and these values were used to calculate the optimum weights for each PMT. The data from each PMT were then used to estimate the energy resolution that would be obtained when the signals from the seven PMT's were summed. This estimate took into account the values of the relative efficiencies, relative PMT gains, and the desired weights for each PMT. Estimates were obtained for both unity weights and the calculated optimal weights.

Using these same data, a correlation matrix between the seven PMT's was also obtained. This was done for each of the five acquisitions, and the mean and standard error of each element in the matrix were obtained.

V. RESULTS

Using only the center tube of the GSPC, pulse height spectra (Fig. 5) were obtained for Xe-133, Am-241, and Tc-99*m*. In the Xe-133 spectrum, three peaks were seen: a total energy peak (81 keV), a fluorescence x-ray escape peak (around 50 keV), and an x-ray peak (around 30 keV), both from the source (cesium x rays) and from the xenon in the detector (fluorescence). In the Am-241 spectrum, the fluorescence x-ray escape peak and the xenon x-ray peak occurred around the same energy (about 30 keV), and the total-energy peak was at 59.5 keV. The Tc-99*m* spectrum contained a total-energy peak (140 keV), a fluorescence x-ray escape peak (110 keV), and a xenon x-ray peak (30 keV). It also contained a peak from lead fluorescence x rays due to photoelectric events in the collimator (around 80 keV) and a corresponding fluorescence x-ray escape peak (around 50 keV). The measurements of energy resolution and the centroid channel number obtained for each peak of interest in these spectra were plotted against energy deposited in Fig. 6. Also shown in this figure is the result of a log–log fit to these data. The slope of this fit is 0.47 ± 0.08.

Energy resolution and the signal value (as measured by the centroid channel number) of the full energy peak of the Am-241 59.5-keV gamma ray were plotted as a function of voltage across the scintillation region in Fig. 7. A least-squares fit to a linear-quadratic equation between the square of the energy resolution data (measured in the absolute units of channel number) and the difference between the scintillation region voltage and the threshold voltage for secondary scintillation [as in Eq. (26)] is also shown in Fig. 7, and was

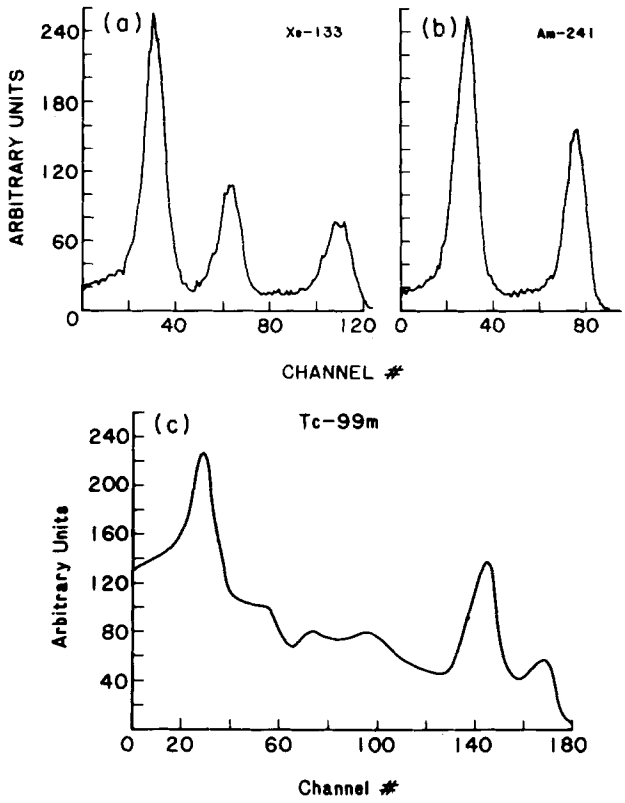

FIG. 5. Pulse height spectra obtained with the GSPC are shown. (a) Xenon-133. The spectrum shows three peaks: an 81-keV photopeak, a 51-keV fluorescence escape peak, and a 30-keV x-ray peak. (b) Americium-241. The two peaks shown are the 59.5-keV photopeak and a 30-keV peak, which is the result of both fluorescence escape and xenon x rays. (c) Technetium-99*m*. The 140-keV photopeak with its associated 110-keV fluorescence escape peak, along with the 30-keV xenon x-ray peak are seen. Also seen in the technetium spectrum are lead fluorescence x rays from the collimator at about 80 keV and a resulting fluorescence escape peak at 50 keV. All of these spectra were collected with a drift voltage of 2.2 kV, scintillation region voltage of 3.0 kV, PMT voltage of 1.45 kV, and integration time of 6 μs. For each spectra, 5×10^4 events were collected and the sum of the signals from all of the PMT's with unity weights was used.

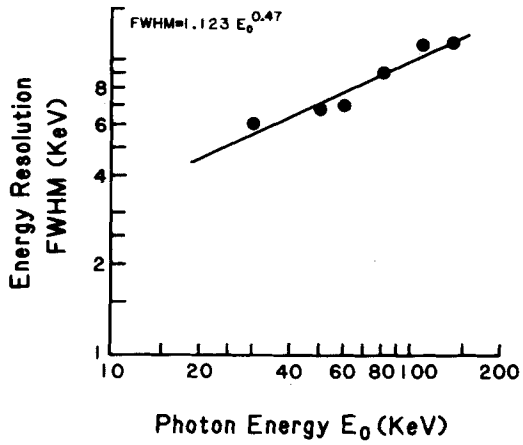

FIG. 6. A log–log plot of the energy resolution data, i.e., the FWHM of the energy peak measured in keV, as a function of peak energy. If the resolution is limited by the number of photons collected, then the resolution data are proportional to the square root of the peak energy. A least-squares fit to the data is also shown, and the expected value of the exponent is 0.47 ± 0.08, which is consistent with theory.

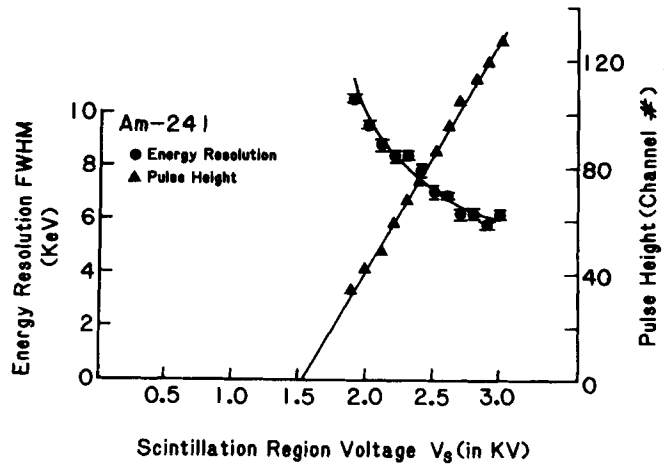

FIG. 7. The energy resolution measured as FWHM in keV of the 59.5-keV photopeak of Am-241 is plotted as a function of voltage across the scintillation region of the chamber. These data are for the signal from the center PMT only. Theory predicted that the energy resolution, measured as FWHM of the photopeak in channel number should be related to the scintillation region voltage by Eq. (26). The results of a least-squares fit of the data to such an equation are shown by the drawn curve and are consistent with the measured data. Also shown is a plot of channel number associated with the centroid of the photopeak as a function of scintillation region voltage, which, as in Fig. 4, is linear with voltage, once above the threshold voltage for secondary scintillation.

seen to be consistent with the measured data. A linear least-squares fit to the centroid data is also presented.

The centroid channel number and energy resolution of the 59.5-keV gamma ray of Am-241 were plotted as a function of drift voltage in Fig. 8. Substantially reduced pulse height and

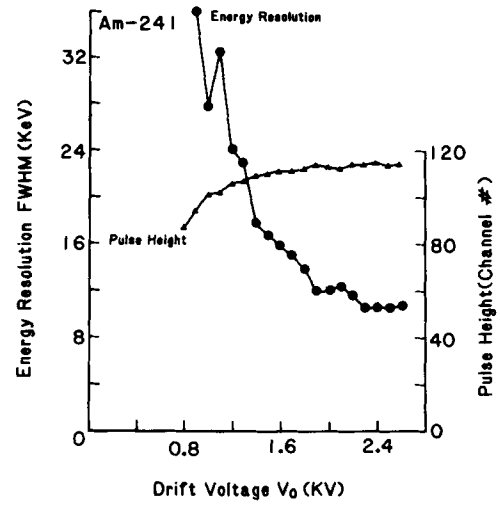

FIG. 8. The energy resolution, measured as the FWHM in keV of the 59.5-keV, is plotted as function of voltage across the drift region of the GSPC. These data were measured from the signal of just the center PMT. Also plotted are the values of the centroid of the peak channel. Energy resolution continues to improve with increasing drift voltage up to 2.3 kV drift voltage. The centroid channel number increases also up to this voltage. Once the drift voltage is above 2.3 kV, the resolution shows no further improvement with increased drift voltage, and the peak channel number does not increase. This is probably because there is no further recombination of the electrons and positive ions once above this voltage. These data were collected with scintillation region voltage of 2.6 kV, PMT voltage of 1.45 kV, and integration time of 5 μs.

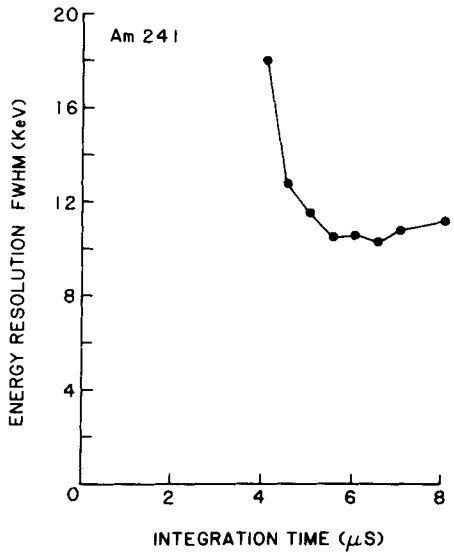

FIG. 9. The energy resolution, measured as the FWHM in keV of the 59.5-keV photopeak of Am-241; is shown as a function of the integration time of the analog-to-digital conversion. The shape of the secondary scintillation pulse was observed on the oscilloscope to be Gaussian-shaped with a FWHM of 2 μs and a FWTM of 5 μs. An optimum integration time of 5.5 μs demonstrated in this figure was consistent with these observations. Shorter integration time does not allow for collection of all the available secondary scintillation photons and longer integration time merely adds noise to the signal. These data were collected with a drift voltage of 2.4 kV, scintillation region voltage of 2.6 kV, and PMT voltage of 1.45 kV.

TABLE I. Values of energy resolution, centroid channel number, relative light gain–efficiency product, relative pulse height, and estimated PMT gain, along with their standard deviations for each of the seven PMT's. These values were obtained from five acquisitions of 20 000 total counts each and the data listed for energy resolution and centroid channel number are the means and standard errors from these five observations. The rest of the data listed were calculated from these values. The relative values were normalized by the value for the center PMT (PMT #1).

PMT #	Energy resolution % FWHM	Signal centroid channel #	$\overline{LT}_{rel}$	$\overline{P}_{rel}$	A_{rel}
1	11.0	589.12	1.000	1.000	1.000
	± 0.4	± 5.84			
2	33.3	121.43	0.114	0.206	1.807
	± 1.1	± 3.22	± 0.011	± 0.006	± 0.182
3	16.8	131.06	0.454	0.222	0.489
	± 0.2	± 1.73	± 0.034	± 0.004	± 0.038
4	36.2	110.39	0.0968	0.187	1.932
	± 1.2	± 1.43	± 0.0091	± 0.003	± 0.184
5	23.2	120.20	0.237	0.204	0.861
	± 0.3	± 2.67	± 0.018	± 0.005	± 0.069
6	24.3	89.74	0.216	0.152	0.704
	± 0.5	± 0.14	± 0.018	± 0.002	± 0.059
7	17.5	151.79	0.418	0.258	0.617
	± 0.3	± 1.16	± 0.033	± 0.003	± 0.049

resolution are demonstrated at drift voltages below 1.5 kV, but this is not the case at 2.2 kV, where the detector is generally operated. The energy resolution of the Am-241 source as a function of the integration time is shown in Fig. 9. The optimal gate duration was 5.5–6 μs.

The means and their standard errors for the energy resolution and the relative pulse height for each PMT are listed in Table I. From these data, the relative light gain–efficiency product was estimated using Eq. (16). Estimates of the relative PMT gain were then obtained. These values are also listed in Table I. Using these values, the estimate for the energy resolution from summing the seven PMT signals with optimum weights was obtained and was 7.31 ± 1.47% FWHM, compared with a measured value with the same weights of 10.9 ± 0.4% FWHM.

The correlation matrix describing the correlation between the PMT's is given in Table II. The element values are the means (with their standard errors) obtained from the five acquisitions.

VI. DISCUSSION

The results shown in Fig. 6 indicated energy resolution values that were superior to those obtained with a NaI detector, at these energies. Increasing photon energy should im-

TABLE II. Correlation matrix between the PMT's of the GSPC. The element values listed are the means of the values for five acquisitions for 20 000 counts each. Also listed are the standard errors of the means. A window was placed around the photopeak for each PMT considered and only counts within this window were used in calculating these values of the correlation coefficient. The values here are substantially higher than would be predicted by Eq. (23), and thus indicate the presence of correlated noise of the form described in Eq. (25).

PMT #	1	2	3	4	5	6	7
1	...	0.179	0.495	0.318	0.320	0.200	0.435
		± 0.008	± 0.010	± 0.005	± 0.006	± 0.008	± 0.004
2	...	...	− 0.015	0.195	0.091	0.494	0.078
			± 0.011	± 0.006	± 0.003	± 0.006	± 0.007
3	...	...	...	0.135	0.340	0.083	0.388
				± 0.005	± 0.006	± 0.008	± 0.004
4	...	...	...	...	− 0.037	0.195	0.250
					± 0.005	± 0.005	± 0.003
5	...	...	...	...	...	0.199	0.074
						± 0.005	± 0.005
6	...	...	...	...	...	...	0.010
							± 0.007
7	...	...	...	...	...	...	...

prove the absolute energy resolution (FWHM measured in keV), which should be related to the square root of the energy deposited for that peak, thus the slope of the log–log plot should be 0.50. The measured value of 0.47 ± 0.08 indicates that these data are consistent with this theory.

If the energy resolution is limited by the number of UV photons collected by the PMT's, increasing the light gain while keeping the energy deposited constant should improve the energy resolution. Figure 7 shows a least-squares fit to a linear-quadratic polynomial to the absolute resolution data (measured in number of channels) and the difference between the scintillation region voltage and the threshold voltage for secondary scintillation, i.e., $V_s - V_{th}$. The value of V_{th} used was obtained from the linear least-squares fit to centroid channel number data in Fig. 7 and was assigned a value of 1.53 kV. This linear-quadratic fit was seen to be consistent with the measured data.

Nguyen Ngoc *et al.*[5] published an estimate of the energy resolution with their GSPC. Their expression was consistent with the formulation presented in this report, in the form of Eqs. (2), (5), and (17), for $K\overline{T}F = 1/9$, where F is the Fano factor (0.15 for xenon) and thus $K\overline{T}$ has a value of 0.654. A value for $K\overline{T}$ of 0.153 at a scintillation region voltage of 2.8 kV was obtained from the energy resolution data presented here and Eq. (16). This indicated that Nguyen Ngoc's device collects four times more light than the GSPC described here. Nguyen Ngoc estimated a light-collection efficiency of 0.009 photoelectrons from the photocathode per photon emitted from the scintillation region. In the device reported here, the scintillation region is located 5.5 cm above the PMT's and is separated from them by a 1.2-cm fused-silica window. The radius of the photocathode of the tube is 2.1 cm. If it is assumed that the phototube has a quantum efficiency of 0.15 (manufacturer's listed value), and that the fused-silica window transmits 50% of the light incident upon it, the light-collection efficiency is given by $\overline{T} = 0.0025$. This is 3.6 times smaller than the $\overline{T}$ assumed for Nguyen Ngoc's device. Adjusting Eq. (34) by increasing the value 9 by a factor of 3.6 to 32.4 to take into account the lower light-collection efficiency, yields an energy resolution value of 9.9% at $V_s = 2.7$ kV and E_0 of 59 keV, which is comparable to the measured value of 10.4%. Thus the experimental data were consistent with that of Nguyen Ngoc's when the difference in light-collection efficiency was taken into consideration.

At low drift voltages, recombination would eliminate electrons from the electron cloud and lead to a loss in both pulse height and energy resolution. Once the drift voltage is sufficient to prevent recombination, a plateau is reached where further increases have little effect. This is true, of course, as long as the drift voltage is well below the level that would lead to excitation of ionization of the fill-gas atoms. This was the case as shown in Fig. 8. Once the drift voltage was above 2.2 kV, there was little improvement with subsequent increases in drift voltage.

Figure 9 indicated that the optimum gate length (or integration time) was about 6 μs. This was consistent with the observation that the pulse duration is approximately 5 μs. Integrating for a shorter period of time will not allow for the collection of all the light, and integrating longer only adds noise to the signal.

The discrepancy between the estimated and the measured variation in the sum signal implies that there is a source of noise that is correlated between the PMT's such that combining their signals does not yield a gain in energy resolution. This is also indicated by the correlation coefficient values of Table II. For PMT #1 and PMT #3, the estimated correlation coefficient from Eq. (23) would be equal to 0.0180 and this would be the largest correlation value between the PMT's. Clearly, the correlation values shown in Table II were due to another source of noise. Taking the calculated value of resolution and adding a covariance term (calculated from the correlation matrix of Table II) to it, as described in Eq. (24), led to an estimate of energy resolution of the sum signal of 11.3%, which was consistent with the measured value.

This correlated noise may be due to 60-Hz noise within the electronics of the detector, caused by a ground loop problem within the data collection system. This noise was not evident in the signal from just the central PMT alone because its magnitude need only be a small fraction of the central PMT signal for it to degrade the resolution of the sum signal. If the magnitude of this correlated noise were equal for all tubes and perfectly correlated, then its value need only be 1% of the central PMT signal for it to lead to the loss of resolution in the sum signal that was experienced.

Other sources of correlated noise that may lead to this degradation of resolution are the reflection of stray scintillation photons within the detector, fluorescence capture within the detector, and light leaks in the PMT array. These noise sources would lead to a geometric variation in the correlation matrix. Examination of the values in Table II indicated that the nearest neighbor PMT's tend to have higher correlation values than the others. Thus the correlated noise may be due to one of these sources.

In order to obtain the sum signal with the best energy resolution, it becomes imperative to control external sources of noise, particularly if this noise leads to a correlation between the PMT's. Because small sources of noise can lead to large losses of energy resolution, it is difficult to improve the resolution by adding the signals from a number of PMT's together. In the case of this GSPC, the energy resolution of the device utilizing all seven tubes was not substantially better than using just the center tube.

ACKNOWLEDGMENTS

We are very grateful to Ron Burns of Xentronics for his help in the construction of the device. We would also like to thank Deborah Hansen for her help with the figures. This research was funded by USPHS Grant No. R01 HL24496.

APPENDIX

As in the text of the paper, the mean electron conversion yield is $\overline{J}$ and the light gain is $\overline{L}$. Neither of these values will depend upon which PMT is collecting the light. However, each PMT will have a different light-collection efficiency and PMT gain and these will be given by $\overline{T}_i$ and $\overline{A}_i$ for the ith

PMT, respectively. When the energy deposition estimate is obtained, each PMT will also be associated with a weight given by w_i. For n PMT's, the sum signal is given by

$$\overline{S}_s = \overline{JL} \sum_{i=1}^{n} \overline{T}_i \overline{A}_i w_i \,. \tag{A1}$$

Using the simplified version of the variance for a single PMT from Eq. (16), the variance of the weighted signal from the ith PMT is

$$\mathrm{var}(S_i) = \overline{JL}^2 \overline{T}_i^2 \overline{A}_i^2 w_i^2 [\, F + (1/\overline{LT}_i)\,] \,, \tag{A2}$$

where F is the Fano factor associated with the fill gas. The covariance between the ith and jth PMT for N data points is

$$CV(S_i,S_j) = \left(\frac{1}{N}\right) \sum_{x=1}^{N} [\,(J_x L_x \overline{T}_i \overline{A}_i w_i - \overline{JLT}_i \overline{A}_i w_i) \times (J_x L_x \overline{T}_j \overline{A}_j w_j - \overline{JLT}_j \overline{A}_j w_j)\,] \,,$$

which reduces to

$$CV(S_i,S_j) = \overline{L}^2 \overline{A}_i \overline{A}_j \overline{T}_i \overline{T}_j w_i w_j F \overline{J} \,. \tag{A3}$$

Utilizing the rule for propagation of errors, an expression for the variance of the sum signal can be obtained:

$$\mathrm{var}(S_s) = \sum_{i=1}^{N} \mathrm{var}(S_i) + 2 \sum_{\substack{i=1 \\ i \neq j}}^{N} \sum_{j=1}^{N} CV(S_i,S_j) \,. \tag{A4}$$

By combining with Eqs. (A2) and (A3), the expressions given in Eqs. (19) and (20) are obtained.

The correlation coefficient between the ith and jth PMT's is

$$r_{ij} = \frac{CV(S_i,S_j)}{[\mathrm{var}(S_i)]^{1/2} [\mathrm{var}(S_j)]^{1/2}} \,.$$

Substituting in the values for $\mathrm{var}(S_i)$ and $CV(S_i,S_j)$ given in Eqs. (A2) and (A3), respectively, yields the expression given in Eq. (23).

[a] Present address: Division of Nuclear Medicine, Georgetown University Hospital, 3800 Reservoir Road, N.W., Washington, DC 20007.

[1] F. H. Fahey, R. E. Zimmerman, R. C. Lanza, and P. F. Judy (in preparation).
[2] F. H. Fahey, R. E. Zimmerman, R. C. Lanza, and P. F. Judy (in preparation).
[3] B. G. Taylor, J. Davelaar, G. Manzo, and A. Peacock, IEEE Trans. Nucl. Sci. **28**, 857 (1981).
[4] A. Peacock, R. D. Andresen, E. A. Leimann, A. E. Long, G. Manzo, and B. G. Taylor, Nucl. Instrum. Methods **169**, 613 (1980).
[5] H. Ngoc Nguyen, J. Jeanjean, H. Itoh, and G. Charpak, Nucl. Instrum. Methods **172**, 603 (1980).
[6] H. Ngoc Nguyen, S. Majewski, G. Charpak, and A. J. P. L. Policarpo, J. Nucl. Med. **20**, 335 (1979).
[7] H. W. Strauss, K. Harrison, J. K. Langan, E. Lebowitz, and B. Pitt, Circulation **51**, 641 (1975).
[8] B. L. Holman, R. E. Zimmerman, L. V. Bifolck, and R. D. Neirinckx, J. Nucl. Med. **20**, 538 (1979).
[9] S. Treves, C. Cheng, A. Samuel, R. Lambrecht, B. Babchyck, R. Zimmerman, and W. Norwood, J. Nucl. Med. **21**, 1151 (1980).
[10] R. N. Beck, M. W. Schuh, T. D. Cohen, and N. Lembares, in *Medical Radioisotope Scintigraphy* (IAEA, Vienna, 1969), Vol. 1, pp. 594–616.
[11] J. C. Ehrardt, L. W. Oberley, and S. C. Lensink, J. Nucl. Med. **15**, 943 (1974).
[12] M. M. Dresser and G. F. Knoll, IEEE Trans. Nucl. Sci. **20**, 266 (1973).
[13] G. Charpak and C. A. Renard, J. Phys. Radium **17**, 585 (1956).
[14] A. J. P. L. Policarpo, Space Sci. Instrum. **3**, 77 (1977).
[15] U. Fano, Phys. Rev. **72**, 26 (1947).
[16] E. P. deLima, M. Salete, S. C. P. Leite, M. A. F. Alves, and A. J. P. L. Policarpo, Nucl. Instrum. Methods **192**, 575 (1982).
[17] H. Silipa, Nucl. Instrum. Methods **133**, 251 (1976).
[18] C. A. N. Conde, L. R. Ferreira, and M. F. A. Ferreira, IEEE Trans. Nucl. Sci. **24**, 221 (1977).
[19] D. E. Cumpstey and D. G. Vass, Nucl. Instrum. Methods **171**, 473 (1980).
[20] G. D. Alkhazov, A. P. Komar, and A. A. Vorobev, Nucl. Instrum. Methods **48**, 1 (1967).
[21] G. F. Knoll, *Radiation Detection and Measurement* (Wiley, New York, 1979), p. 283.
[22] R. L. Richardson, in *Nuclear Medicine Physics, Instrumentation, and Agents*, edited by F. D. Rollo (Mosby, St. Louis, 1977), pp. 231–270.